Calculation of IES Moments (level 5) from Differential Energy Flux (level 3) data product

K. LLera, P. Mokashi and the IES Archiving Team

1. Scope

The purpose of this document is to provide the algorithms and quantities needed to convert the differential energy flux from level 3 data into three moments: density, velocity, and temperature for the mass and charge of the observed particles. Due to the inherent discrete nature of the instrument, the moments are calculated by the discrete sum.

2. Species identification

The IES instrument measures E/q and therefore, the mass of detected particles is unknown. We designate a mass and charge based on the known characteristics of the solar wind. If multiple species are observed as discrete and separable E/q signals over time, they are identified in relation to the solar wind proton signal. Identification of negative ions is also designated in relation to the ion detector's solar wind proton signal. If we are unable to designate a mass and charge for observed data, such as for cometary ions, the moments are not calculated. Different electron populations (solar wind, cometary, etc.) are not separated in the moments data files.

3. Plasma distribution moments

The level three data product is the derived differential energy flux (DEF):

$$DEF = \frac{(C / \Delta t)'}{G * \varepsilon}$$

(1)

where the instrument counts C depend on the cycle duration Δt, the geometric factor G and the detector efficiency ε. These are discussed in the level 3 document, FLUX_CALCULATION.PDF. The apostrophe in Equation 1 denotes the measurement is background subtracted. The *DEF* is multiplied by 1×10^{-4} to convert to centimeters and resulting in units of *particles/(cm² s sr eV/eV)*.

To conduct moment equations, the velocity space density is first derived from DEF as shown in Equation 2:

$$f_{i,j,k,s} = \frac{DEF_{i,j,k,s} * m_s^2}{2 E_k^2} = \frac{2 * DEF_{i,j,k,s}}{v_{k,s}^4}$$

(2)

where $f_{i,j,k,s}$ is the velocity distribution function $f_s(v)$ for each species s, energy *E*, and mass m_s. Depending on the equation, the constants and conversion factors needed are described below. For the velocity equation substituted by the kinetic equation, the value of

E_k is in *eV,* the value of m_s is in AMU and multiplied by $1.0453453\text{x}10^{-12}$ *eV s²/AMU cm²* to obtain the standard units for $f_{i,j,k,s}$ in $cm^{-6}s^3$. The *ijk-* indices denote the azimuth, elevation, and energy dependence respectively. The methods used to compute the moments from this distribution will be discussed in the following sections.

3.1 Number density (n_s)

The number density of positively or negatively charged species *s* is determined by performing the following operation on the velocity distribution function, $f_{i,j,k,s}$:

$$n_s = \sum_{k=0}^{123} v_k^2 * (v_{k+1} - v_k) \sum_{i=0}^{15} \alpha_i \sum_{j=0}^{15} \cos(\bar{\beta}_j) * \beta_j * f_{i,j,k,s}$$

(3)

where *k* is the energy step index, *i* is the azimuthal index, *j* is the elevation index, and n_s is in units of cm^{-3}. The velocity values v_k and v_{k+1} are determined from the energy range between *k* and *k+1* energy steps and the mass of the respective species *s*. The kinetic energy (Equation 4) is used to obtain the velocity for mass *m* given in AMU and energy *E* given in eV:

$$v_k = \sqrt{\frac{E_k}{b * m_s}} * 10^5$$

(4)

where *b* is a constant with a value of 0.005182. A conversion factor of $1\text{x}10^5$ is used to obtain standard units for velocity, *cm s⁻¹*. α_i is the ith azimuth look direction in radians. $\bar{\beta}_j$ is the midpoint of the jth elevation anode in radians.

Each species *s* appears as enhanced flux confined in energy, azimuth, and elevation bins; restricting the *ijk*-indices into a select range for the moment equations. Filtering of the energy, azimuth, and elevation ranges to calculate the moments is discussed in section 4.

3.2 Velocity (u_s)

The velocity is calculated by first computing the velocity components.

$$u_s = u_{x,s}\hat{i} + u_{y,s}\hat{j} + u_{z,s}\hat{k}$$

(5)

The components are calculated as follows:

$$u_{x,s} = \frac{1}{n_s}[\sum_k v_k^3 * dv \sum_i \cos(\alpha_i) * \alpha_i \sum_j \cos(\bar{\beta}_j)^2 * \beta_j * f_{i,j,k,s}]$$

(6)

$$u_{y,s} = \frac{1}{n_s}[\sum_k v_k^3 * dv \sum_i \sin(\alpha_i) * \alpha_i \sum_j \cos(\bar{\beta}_j)^2 * \beta_j * f_{i,j,k,s}]$$

(7)

$$u_{z,s} = \frac{1}{n_s}[\sum_k v_k^3 * dv \sum_i \alpha_i \sum_j \sin(\bar{\beta}_j)*\cos(\bar{\beta}_j)*\beta_j * f_{i,j,k,s}]$$

(8)

where dv is the energy range of E_k and u_s is in units of $cm\ s^{-1}$ and then converted to $km\ s^{-1}$ in all level 5 products.

The reported velocities are converted from the instrument coordinates into Comet-centered Solar Equatorial coordinate system (CSEQ). CSEQ is oriented with the comet body at its origin and the x-axis pointing towards the Sun. The z-axis points along the part of the solar north pole that is orthogonal to the x-axis and the y-axis completes the right-handed coordinate system.

The scalar bulk velocity is reported by taking the magnitude of u_s, $||u_s||$.

3.3 Scalar temperature (T_s)

This scalar moment is obtained from the trace of the temperature tensor,

$$\left\|T_s\right\| \equiv Tr(T_s)/3 = T_{xx,s} + T_{yy,s} + T_{zz,s}.$$

(9)

The diagonal components of the temperature tensor are determined from the pressure relation expressed as:

$$\frac{Tr(T)}{3} = \frac{Tr(P)}{3*n_s*k_B}$$

(10)

The pressure tensor is expressed in terms of the velocity relative to the bulk velocity, u_s:

$$T_{xx,s} = \frac{m_s}{3*k_B*n_s}[\sum_k v_{k,s}^2 * dv \sum_i \alpha_i \sum_j \cos(\bar{\beta}_j)*\beta_j *(v_{k,s}*\cos(\alpha_i)*\cos(\bar{\beta}_j)-u_{xx,s})^2 * f_{i,j,k,s}]$$

(11)

$$T_{yy,s} = \frac{m_s}{3*k_B*n_s}[\sum_k v_{k,s}^2 * dv \sum_i \alpha_i \sum_j \cos(\bar{\beta}_j)*\beta_j *(v_{k,s}*\sin(\alpha_i)*\cos(\bar{\beta}_j)-u_{yy,s})^2 * f_{i,j,k,s}]$$

(12)

$$T_{zz,s} = \frac{m_s}{3*k_B*n_s}[\sum_k v_{k,s}^2 * dv \sum_i \alpha_i \sum_j \cos(\bar{\beta}_j)*\beta_j *(v_{k,s}*\sin(\bar{\beta}_j)-u_{zz,s})^2 * f_{i,j,k,s}]$$

(13)

where k_B is the Boltzmann constant. From the diagonalized tensor components, the scalar tensor is determined by summing these three equations in units of Kelvin.

4. Filtering for each species

The IES detectors generally observe particles originating from both the solar wind and the comet. Filtering flux data in energy, azimuth, and elevation improves the moment calculations given our single species assumption. If multiple species are evident, we repeat the process (Equations 1-13) for each species where we can designate a mass and charge.

The summation is collapsed to include only the *i j k*-indices contributing to that species *s* as follows,

$$n_s = \sum_{k_{mn}}^{k_{mx}} v_k^2 * (v_{k+1} - v_k) \sum_{i_{mn}}^{i_{mx}} \alpha_i \sum_{j_{mn}}^{j_{mx}} \cos(\bar{\beta}_j) * \beta_j * f_{i,j,k,s}$$

(14)

where the *mn* and *mx* subscripts for the *ijk*-summations indicate the minimum and maximum step where the species is observed.

Over time, the ranges may shift due to a spacecraft maneuver or the dynamic solar and cometary environment. The ranges for the *ijk*–indices are accordingly varied.

We take the following steps to filter the data.

4.1 Energy range

Solar wind populations detected by IES (E/Q measurement) have been observed as narrow banded energies. Therefore, the energy range is determined first. We select the *k*-indices that bound the particular energy band throughout a day of data and designate a mass and a charge. Any data outside this range is not included in the moment calculations for that species.

For electrons, separation of species of different origins is not possible with a high degree of confidence, so the entire observed range is selected.

4.2 Azimuth range

The next filtered parameter is the azimuthal look direction. Particles arriving from the comet or from the solar wind direction appear at different azimuth sections. By plotting only the flux within the energy range selected, the azimuthal direction of the detection becomes unambiguous. This min and max of the range are selected for i-indices.

4.3 Elevation range

With both the energy and azimuth filters applied, the elevation data show flux clearly for the sought out species *s*. The min and max are then selected for *j*-indices. For electrons, the range may be most of the instrument range while ions the range may narrow.

5. Quality control

To ensure confidence in generated moments, we employ two methods – exclusion of very low confidence data that are not physically realistic and use of quality flags.

5.1 Data exclusion

Data collected by the instrument when the MCP voltage was not nominal are excluded. The MCP voltage quality flag from level 3 data products is used to identify such periods.

An internal quality test has resulted in removal of data when densities are below a threshold level. Below this level, the calculated velocity and temperature moments are not physically realistic. Removing these low densities improves the overall moments and statistics. An example is provided in Section 7. Threshold levels for the different species are listed in Table 1.

Table 1: Threshold Densities	
Species	**Threshold Level (n cm^{-3})**
Protons	0.002
Heavier positive ions	0.001
Electrons	0.0004
Heavier negative ions	0.001

We also do not create moment files if there are less than 10 data points for a day.

5.1 Quality flags

The moment text files have a quality flag column designated to inform the user of data concerns and whether the species assumptions are not optimum. Currently, one new quality flag and two level 3 data flags are displayed when applicable. The flags are described below.

5.1.1 Peak on the edge of FOV

This flag denotes time intervals in which the bulk of the distribution may be outside of the field of view (FOV). This is determined by testing whether at least 80% of the differential flux peak is at the edge of our spatial coverage. For both the ion and electron sensors, the IES field of view is limited in the elevation range. Additionally, due to the removal of noisy anodes in the electron sensor, a limitation exists with respect to azimuth bins. Therefore, from the filtered ranges and for all moments, we check whether at least 80% of the peak is within elevation anode(s) 0 or 15. The electron sensor also checks if this criteria is met in azimuth anode(s) 10 or 13.

5.1.2 Possible ICA interference

This quality flag from level 3 data is also used in level 5 data to identify the time intervals where ICA interference is possible in the electron sensor. In level 5 data, this quality flag is in position two for negatively charged species and set to 1 during those intervals.

5.1.3 Possible light contamination

This quality flag from level 3 data is also used in level 5 data to identify the time intervals where noise from a possible light leak is detected in the ion sensor. In level 5 data, this quality flag is in position two for positively charged species and set to 1 during those intervals.

6. Caveats

6.1 Spacecraft Potential

The spacecraft (S/C) potential is determined by the imbalance between negative and positive currents at the S/C. In the undisturbed soar wind, this imbalance is determined by the photoemission of electrons resulting in a positive potential. In the presence of a dense enough plasma, the potential is determined by the density and temperatures of the components. Measurements by the Langmuir probe (LAP) and Mutual Impedance Probe (MIP) on board Rosetta have shown that the S/C potential is negative most of the time, with a magnitude in the order of 10 - 20 Volts. Such a negative potential has the effect of accelerating positively charged particles and decelerating or repelling negative ones. In both cases the measured energy distribution is distorted from the true energy. For solar wind ions of the order of 1 keV or higher, this effect is negligible, but lower energy cometary ions can be affected. Likewise, low energy electrons are also affected.

None of the IES data products have been corrected for spacecraft charging effects. A detailed discussion of the effects of S/C charging is given in Galand et al., (2016), as well as in the RPC_USER_GUIDE.

6.2 Electron populations

Users of RPC-IES level 5 data should proceed with caution and understanding that different electron populations are not separated in the moments data files.

The electrons measured by RPC-IES near comet 67P coma consist of several populations from different sources. The quiet solar wind typically contributes 3 separate populations (the core, halo, and strahl). Transients in the solar wind contribute other distributions. Photoionization of material from the comet nucleus produces other populations and electron collision ionization produces more electrons. These populations interact and blend with each other, producing a complicated mess. In addition, the spacecraft is generally charged negatively, typically the order of 10-20 V, resulting in an apparent distortion of the distributions when measured by a Rosetta-based instrument. Another important aspect that may occasionally affect the quality of the data is due to the IES field of view (FOV) being ~2.8 pi, not covering all of space. The result is that as the spacecraft

turns, IES may see different electron populations during the course of the turn. This is not significant for solar wind protons since they are normally either in or out of the FOV.

Several investigators have studied the electron distribution in detail using IES electron data (Clark et al., 2015, Broiles et al., 2016, Madanian et al., 2016) and shown the complexity of these distributions. Separating the populations into individual distributions over the whole mission is a task beyond the funding and time available to the IES team and therefore the level 5 files contain unseparated electron populations.

Users of RPC-IES electron moments data should have an understanding of this issue and proceed with caution.

6.3 Density disparity

The electron densities given in the archive files while Rosetta was near the comet are higher than the solar wind proton densities because they include electrons resulting from the photo-ionization of the cometary neutrals. Generally, the density of photo-electrons is much larger than the density of solar wind electrons and it is not possible to separate the two populations. Thus the total electron densities are greater than that of the solar wind protons.

6.4 Temperature disparity

The mean ratio of the solar wind electron to proton temperature at 1 AU from the Sun is ~2 [Jursa, 1985]. However, the ratio observed in IES data is < 1. We believe the reason for this is that in the coma, the solar wind electrons are cooled by collisions with the neutral atoms lowering the bulk temperatures.

7. Example

In this section, we show an example showing the steps to generate level 5 moments from level 3 data. On 16 April 2016, IES detected solar wind protons, alphas, and cometary ions. The level 3 flux is shown in Figure 1, before any filtering is applied for the moments calculation.
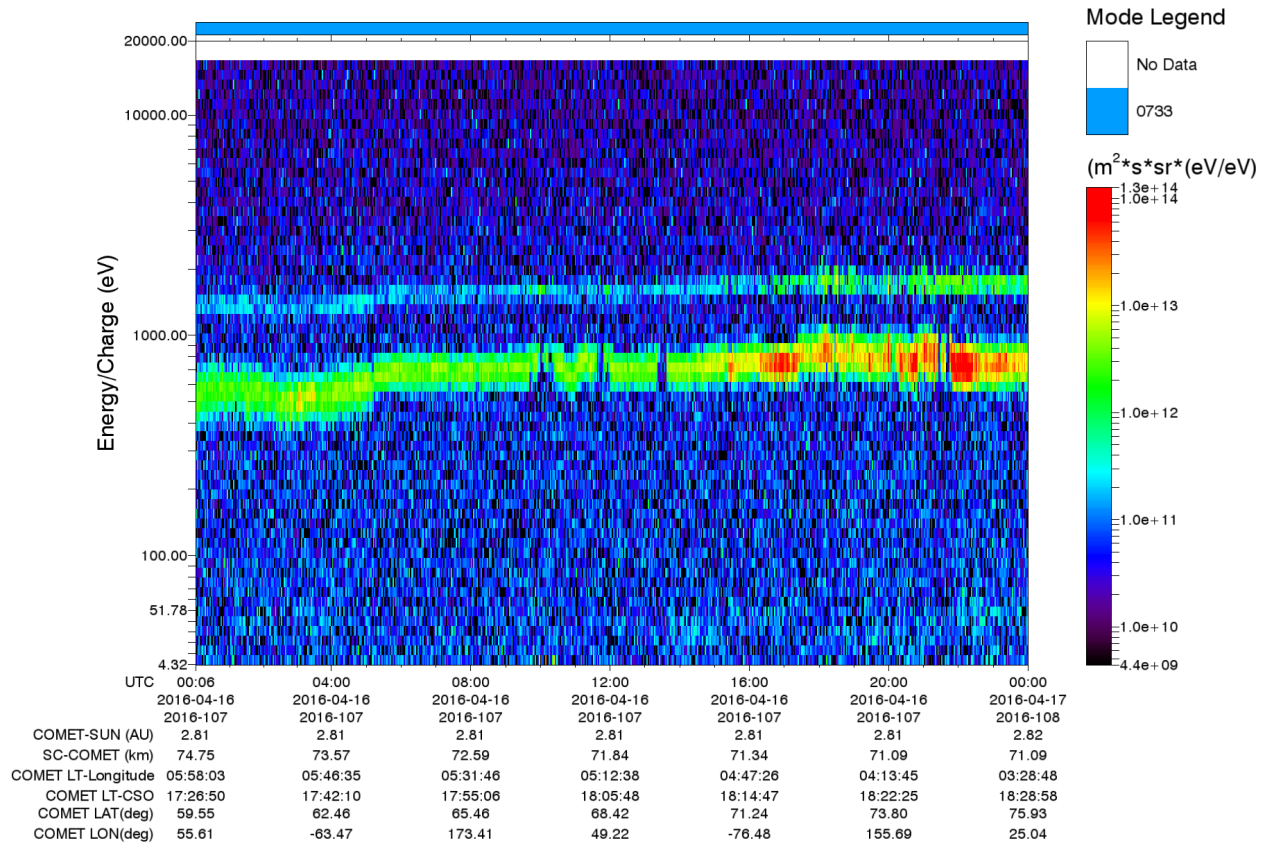
Figure 1. Level three data summed over all azimuth and elevation anodes. The first parameter filtered for the moments code is the energy range, followed by the azimuth and then elevation.

An initial filter is applied to isolate the intended species. Generally, the most constraining parameter is energy. The zero-order filters applied to data shown in Figure 1 for this example are shown in Table 2.

16 April 2016 (DOY-107)		
Initial IES level 3 filters applied for the solar wind protons		
Parameter	Min	Max
Energy [eV]	185.55	1104.66
Azimuth [anode]	1	14
Elevation [anode]	0	15

Table 2. A typical zero-order filter is an energy range bounding the targeted species on the given day. Depending on the azimuthal and elevation plots a more constrained range is applied; as necessary to single out the targets species.

From these plots, a trace is recorded to define the min and max ranges of the targeted species. The selection criterion was to contain the bulk of the distribution. With the DEF

displayed in a log-scale, the filtered ranges contain the peak and the surrounding area with high flux. We determined the high flux to be 2-3 orders of magnitude from the peak, as shown in Figure 2. For each data timestamp, the range filters (i.e., *ikj*-indices) are recorded in a trace file. The moments are then calculated with the level 3 data within the filtered ranges.
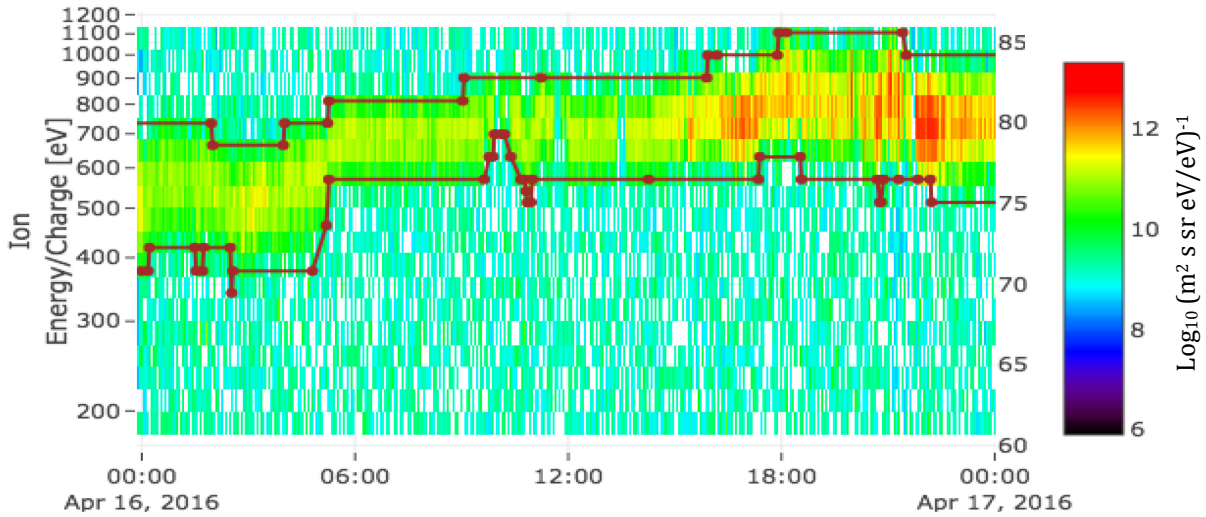
Figure 2. An example of the energy filter selection and tracing shown for 16 April 2016 for Level 3 data. From the reddish-brown line, the min and max energy indices are recorded for each timestamp.

Once the moments are calculated, a final sampling filter is applied as described in section 5.1. We used the density as a proxy for the intervals with low signal to noise data. Figure 3 shows which points meet the exclusion criteria for solar wind protons on 16 April 2016.

After the removal of low-density intervals, if there are at least 10 points remaining within one day of data, we include the moments in the output files.
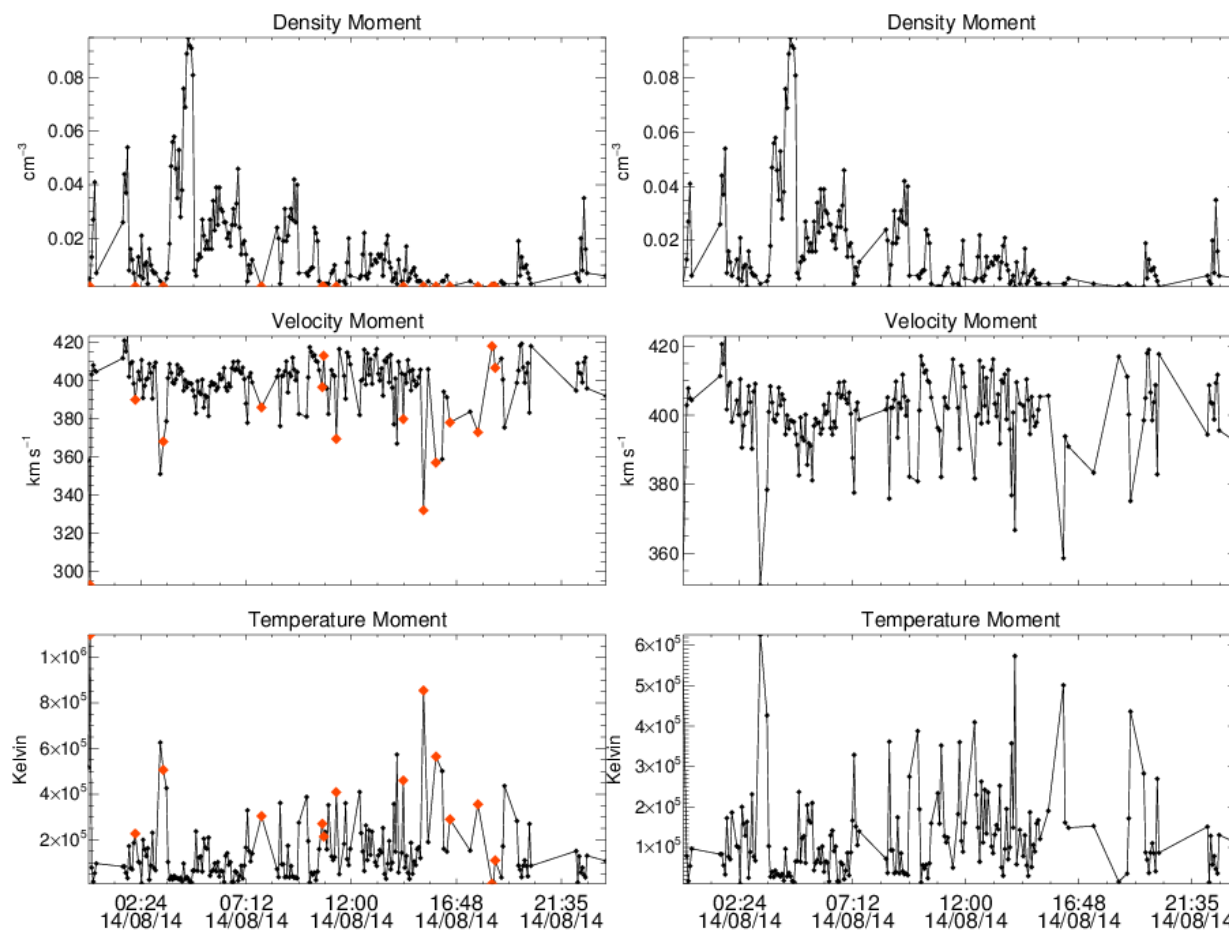
Moments for 2014-226. Assumed Mass=1 amu and Charge=1 q.

Over-plotted are red diamonds, denoting the time intervals in which the density is below the threshold described in section 5.1. The right three panels show only the data above the threshold. Note: The y-axis range has changed for the right three panels.

7. References

M. Galand, et al. (2016), Ionospheric plasma of comet 67P probed by Rosetta at 3 au from the Sun, *Monthly Notices of the Royal Astronomical Society*, *462*, doi: 10.1093/mnras/stw2891

Clark, G. ., et al. (2015), Suprathermal electron environment of comet 67P/Churyumov-Gerasimenko: Observations from the Rosetta Ion and Electron Sensor, *Astronomy & Astrophysics*, 583, doi:10.1051/0004-6361/201526351.

Broiles, T. W., et al. (2016), Characterizing cometary electrons with kappa distributions, *J. Geophys. Res. Space Physics*, 121, 7407–7422, doi:10.1002/2016JA022972.

Madanian, H., et al. (2016), Suprathermal electrons near the nucleus of comet 67P/Churyumov-Gerasimenko at 3 AU: Model comparisons with Rosetta data, *J. Geophys. Res. Space Physics*, 121, 5815–5836, doi:10.1002/2016JA022610.

Jursa, A. S. et al. (1985), Handbook of geophysics and the space environment (Vol. 1), *Air Force Geophysics Lab.*, Hanscom AFB, MA. doi: unavailable